AMERICAN SOCIETY FOR MICROBIOLOGY | Molecular and Cellular Biology®

RESEARCH ARTICLE

Acetylation of Cavin-1 Promotes Lipolysis in White Adipose Tissue

Shui-Rong Zhou, Liang Guo, Xu Wang, Yang Liu, Wan-Qiu Peng, Yuan Liu, Xiang-Bo Wei, Xin Dou, Meng Ding, Qun-Ying Lei, Shu-Wen Qian, Xi Li, Qi-Qun Tang

Key Laboratory of Metabolism and Molecular Medicine, Ministry of Education, and Department of Biochemistry and Molecular Biology, Fudan University Shanghai Medical College, Shanghai, People's Republic of China

ABSTRACT White adipose tissue (WAT) serves as a reversible energy storage depot in the form of lipids in response to nutritional status. Cavin-1, an essential component in the biogenesis of caveolae, is a positive regulator of lipolysis in adipocytes. However, molecular mechanisms of cavin-1 in the modulation of lipolysis remain poorly understood. Here, we showed that cavin-1 was acetylated at lysines 291, 293, and 298 (3K), which were under nutritional regulation in WAT. We further identified GCN5 as the acetyltransferase and Sirt1 as the deacetylase of cavin-1. Acetylation-mimetic 3Q mutants of cavin-1 augmented fat mobilization in 3T3-L1 adipocytes and zebrafish. Mechanistically, acetylated cavin-1 preferentially interacted with hormone-sensitive lipase and recruited it to the caveolae, thereby promoting lipolysis. Our findings shed light on the essential role of cavin-1 in regulating lipolysis in an acetylation-dependent manner in WAT.

KEYWORDS WAT, cavin-1, acetylation, HSL, lipolysis

Received 8 February 2017 **Returned for modification** 6 March 2017 **Accepted** 19 May 2017

Accepted manuscript posted online 30 May 2017

Citation Zhou S-R, Guo L, Wang X, Liu Y, Peng W-Q, Liu Y, Wei X-B, Dou X, Ding M, Lei Q-Y, Qian S-W, Li X, Tang Q-Q. 2017. Acetylation of cavin-1 promotes lipolysis in white adipose tissue. Mol Cell Biol 37:e00058-17. https://doi.org/10.1128/MCB.00058-17.

Address correspondence to Qi-Qun Tang, qqtang@shmu.edu.cn.

White adipose tissue (WAT) plays a critical role in regulating energy homeostasis, mostly by serving as a reversible energy storage depot in the body. Adipocytes store excess energy in the form of triglycerides (TAG), which can be hydrolyzed during nutrient shortage to release free fatty acids (FFA) and glycerol into circulation (1). Obesity is now epidemic and is accompanied by two dramatic effects on adipocyte function, a decrease in TAG synthesis and an increase in lipolysis (2). Abnormalities in the storage and utilization of TAG in WAT lead to high circulating plasma FFA levels, which promotes reesterification of lipids in other tissues (such as the liver) and exacerbates insulin resistance. This underscores the role of lipid metabolism in the pathogenesis of metabolic disorders, such as nonalcoholic fatty liver disease, type 2 diabetes, and atherosclerotic heart disease (3).

Caveolae are small, omega-shaped invaginations of the plasma membrane of many cell types. Caveolae are especially abundant in adipocytes, and they play an important role in lipid trafficking and metabolism (4). Cavin-1, a conserved caveola coat protein required for caveola formation and function, also is involved in the regulation of lipid metabolism (5, 6). Human cavin-1 mutations have been reported in patients with congenital generalized lipodystrophy (7–13). Cavin-1$^{-/-}$ mice have diminished adipose depot mass and smaller fat cells in WAT than wild-type (WT) mice, and *in vitro* cavin-1 null adipocytes display reduced lipolysis and fatty acid uptake and incorporation into lipids compared to WT adipocytes (14). Specific gain- and loss-of-function phenotypes of cavin-1 reveal its role as a positive regulator of lipolysis in 3T3-L1 adipocytes (15). However, molecular mechanisms by which cavin-1 promotes lipolysis in white adipocytes remain poorly understood. Several phosphorylation sites in the cavin-1 protein have been previously identified, and mutations of certain cavin-1 phosphorylation sites (S42A, T304A, or S368A) suppress lipolysis in 3T3-L1 adipocytes, owing to an associated

reduction in hormone-sensitive lipase (HSL) phosphorylation at serine 563 and serine 660 (15, 16). Cavin-1 deficiency has no effect on HSL phosphorylation but substantially reduces perilipin phosphorylation (14). Thus, the functional significance of cavin-1 in the modulation of lipolysis needs to be further characterized.

Reversible lysine acetylation has emerged as a key mechanism to alter protein function for metabolic regulation in response to environmental changes (17). In this study, we employed mass spectrometry (MS)-based proteomic analyses to characterize the acetylated proteins in adipose tissue. We observed that cavin-1 protein was acetylated at three lysine residues: K291, K293, and K298 (3K). Acetylated cavin-1 promoted lipolysis in 3T3-L1 adipocytes, and transgenic zebrafish overexpressing acetylation-mimetic 3Q mutants showed more rapid fat mobilization than those overexpressing WT cavin-1. Therefore, we have uncovered a mechanism whereby 3K acetylation of cavin-1, modulated by nutritional status, promotes lipolysis. Our observations also provide insights into the pathological role of cavin-1 acetylation in obesity-associated metabolic disorders.

RESULTS

Acetylation of cavin-1 at lysines 291, 293, and 298. To identify novel functions of protein acetylation in adipose tissue, we employed MS-based proteomic analyses to evaluate the acetylated proteins. Our approach was based on previously reported protocols (18). Briefly, we separated the different cellular fractions from subcutaneous adipose tissue (SAT), visceral adipose tissue (VAT), and brown adipose tissue (BAT). The proteins in each fraction were digested into peptides with sequencing-grade trypsin. We next used acetyl-lysine antibody affinity purification and MS to characterize several acetylated proteins (see Table S1 in the supplemental material). Acetylated proteins that are highly expressed in adipose tissue, including cavin-1 (also called PTRF, as indicated in Table S1), were particularly interesting to us because of their special functions in lipid metabolism. Tandem MS analysis identified three specific acetylation sites of cavin-1, namely, K291, K293, and K298, which are evolutionarily conserved among species (Fig. 1A). After immunoprecipitation (IP) of cavin-1, Western blotting with an anti-acetyl-lysine antibody confirmed that cavin-1 was indeed acetylated (Fig. 1B), and its acetylation was increased by the treatment of cells with deacetylase inhibitors nicotinamide (NAM) and trichostatin A (TSA) (Fig. 1C). We singly mutated each lysine to an arginine (K291R/K293R/K298R) or generated triple R mutants of all three lysines (3R) and found that all four mutations resulted in a significant reduction in cavin-1 acetylation (Fig. 1D). These findings demonstrate that these three lysine residues are acetylated or deacetylated at the same time and that they are the major acetylation sites of cavin-1.

To further confirm and improve the detection of acetylation of the three lysine residues, we generated an antibody specific for K291, K293, and K298 of cavin-1 (anti-3K-Ac). To characterize the specificity of this antibody, we performed Western blotting to detect the 3K acetylation of ectopically expressed WT cavin-1 in HEK293T cells. The anti-3K-Ac antibody readily recognized cavin-1 during preincubation with and without the unmodified antigen peptides but not with the acetylated 3K-Ac peptides (Fig. 1E). The antibody also detected WT cavin-1 but not 3R (lysine 291/293/298 to arginine) or 3Q (lysine 291/293/298 to glutamine) mutants (Fig. 1F). Interestingly, 3K acetylation of endogenous cavin-1 in 3T3-L1 adipocytes was significantly elevated after treatment with NAM, which is an inhibitor of the sirtuin family of deacetylases, but not by TSA, which is an inhibitor of histone deacetylase (HDAC) classes I, II, and IV (Fig. 1G). These characterizations demonstrate the specificity of our anti-3K-Ac antibody for recognizing 3K-acetylated cavin-1.

NAM increases cavin-1 acetylation and sirt1 is the deacetylase of cavin-1. Deacetylation is regulated by HDACs, which is a class of enzymes that remove acetyl groups from an ε-*N*-acetyl lysine amino acid on a target, including histone and nonhistone proteins (19). Class III HDACs are NAD (NAD^+)-dependent proteins known as sirtuins (Sirt1-7), which are preferentially involved in the deacetylation of nonhistone

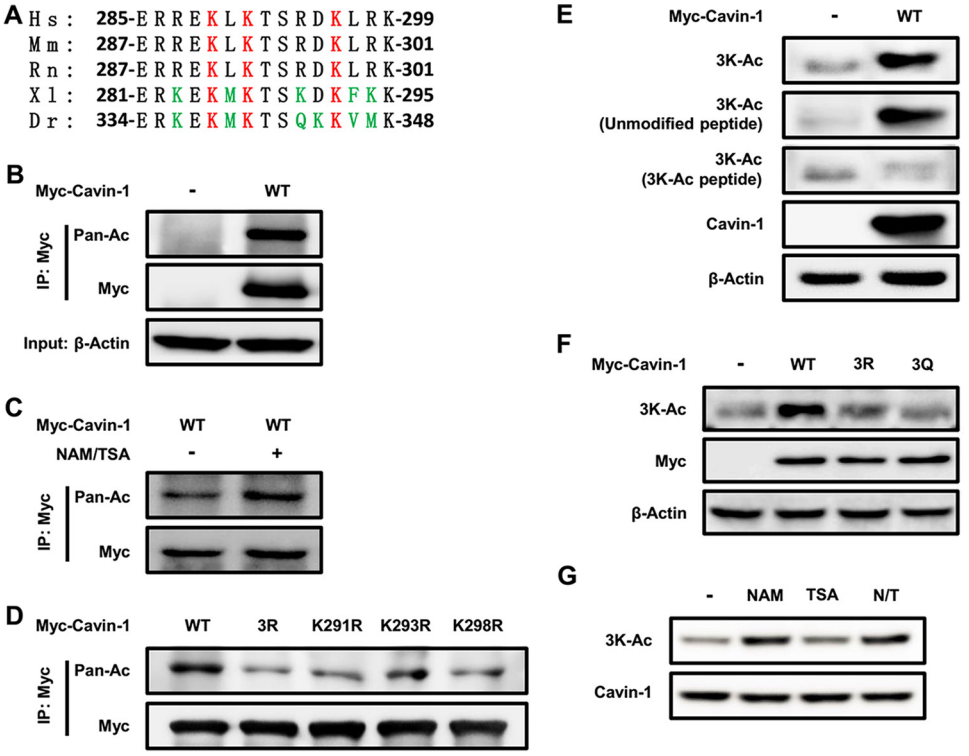

FIG 1 Acetylation of cavin-1 at lysines 291, 293, and 298. (A) The identified acetylated K291, K293, and K298 (Ac-3K) in cavin-1 are conserved. Multiple alignments of the protein sequences around 3K (lysines 291, 293, and 298)-acetylated sites of cavin-1 identified by mass spectrometry from different organisms. Hs, *Homo sapiens* (human); Mm, *Mus musculus* (mouse); Rn, *Rattus norvegicus* (Norway rat); Xl, *Xenopus laevis* (African clawed frog); Dr, *Danio rerio* (zebrafish). (B and C) Exogenous cavin-1 is acetylated. Myc-tagged cavin-1 was transfected into HEK293T cells with or without nicotinamide (NAM) and trichostatin A (TSA) treatment and immunoprecipitated for acetylation analysis by Western blotting with either an anti-pan-acetyl lysine or an anti-Myc antibody. (D) Mutation of K291, K293, K298, or 3K decreases cavin-1 acetylation. HEK293T cells were transfected with the indicated plasmids, and cavin-1 acetylation and protein levels were analyzed by Western blotting with the indicated antibodies. (E and F) The anti-3K-Ac antibody is specific for K291, K293, and K298 of cavin-1. (E) The indicated plasmids were transfected into HEK293T cells. The specificity of the anti-3K-Ac antibody was determined by Western blotting; the antibody was preincubated with or without antigen peptides (acetyl-3K peptide or unmodified peptide). (F) Acetylation of Myc-tagged cavin-1^{WT}, cavin-1^{3R}, and cavin-1^{3Q} was measured by Western blotting with an anti-3K-Ac antibody. (G) NAM, but not TSA, increases 3K acetylation of cavin-1. 3T3-L1 adipocytes were left untreated or were treated with sirtuin deacetylase inhibitor NAM and histone deacetylase inhibitor TSA. Acetylation of endogenous cavin-1 was determined by Western blotting with an anti-3K-Ac antibody. N/T, treated with NAM and TSA.

proteins and emerging as key metabolic sensors (20). To further confirm whether sirtuins are the deacetylase of cavin-1, as shown in Fig. 1G, we ectopically expressed Myc-tagged cavin-1 in HEK293T and treated the cells with NAM. NAM treatment increased cavin-1 acetylation levels in dose- and time-dependent manners (Fig. 2A and B). We next coexpressed cavin-1 with each member of the sirtuin family (Sirt1-7) and found that Sirt1, but not other sirtuins, decreased cavin-1 acetylation (Fig. 2C). Western blotting with anti-3K-Ac antibody barely detected the signal of acetylated cavin-1 by overexpression of WT Sirt1. In contrast to WT Sirt1, catalytically inactive (HY) mutant Sirt1 failed to decrease the acetylation level of cavin-1 (Fig. 2D). Furthermore, Sirt1 knockdown in 3T3-L1 adipocytes resulted in increased acetylation of endogenous cavin-1 (Fig. 2E). In order to explore whether cavin-1 physically interacts with Sirt1, we performed coimmunoprecipitation experiments and found that cavin-1 readily coprecipitated Sirt1 but not Sirt2 (Fig. 2F and G). Taken together, these results indicate that Sirt1 is the deacetylase of cavin-1.

GCN5 enhances cavin-1 acetylation. To identify the lysine acetyltransferase that acetylates cavin-1 at 3K, we individually transfected HEK293T cells with one of four classical acetyltransferases: CBP (CREB-binding protein), p300 (E1A-binding protein, 300

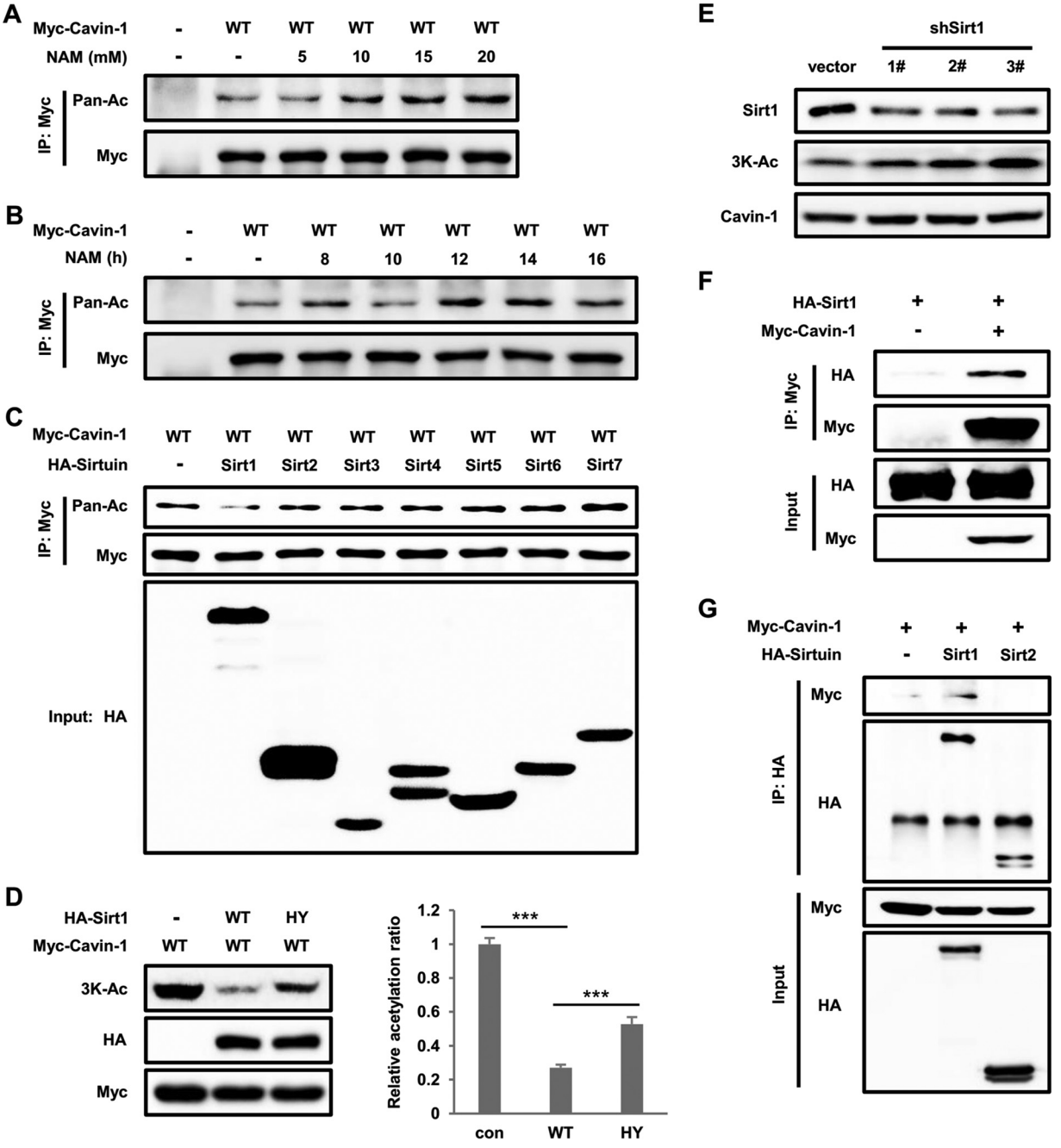

FIG 2 Nicotinamide (NAM) increases cavin-1 acetylation and Sirt1 is the deacetylase of cavin-1. (A and B) NAM increases cavin-1 acetylation levels. Myc-tagged cavin-1 was transfected into HEK293T cells treated with NAM for the indicated concentrations (A) and times (B); the cells were immunoprecipitated using an antibody against Myc. Cavin-1 acetylation levels were assessed with an anti-pan-acetyl lysine antibody. (C) Overexpression of Sirt1 decreases cavin-1 acetylation. Myc-tagged cavin-1 was cotransfected with HA-tagged members of the sirtuin family (Sirt1-7) into HEK293T cells. Cavin-1 acetylation and protein expression were determined by Western blotting with the indicated antibodies. (D) Catalytic activity of Sirt1 is responsible for the deacetylation of cavin-1 at 3K. Myc-tagged cavin-1 was cotransfected with HA-tagged wild-type (WT) or catalytically inactive mutant (HY) Sirt1 into HEK 293T cells. Acetylation of cavin-1 was measured by Western blotting with an anti-3K-Ac antibody. Relative acetylation/protein ratios were quantified. con, cotransfected with vector control; WT, cotransfected with wild-type Sirt1; HY, cotransfected with catalytically inactive mutant Sirt1. Error bars represent ±SD for experiments performed in triplicate. (E) Sirt1 knockdown increases endogenous cavin-1 acetylation levels. 3T3-L1 adipocytes were infected with lentivirus-driven shSirt1 or control shRNA, and endogenous cavin-1 acetylation at 3K was measured by Western blotting. (F and G) Sirt1 interacts with cavin-1. The indicated plasmids were transfected into HEK293T cells. The interaction between Sirt1 and cavin-1 was detected by immunoprecipitation and Western blotting.

kDa), GCN5 (lysine acetyltransferase 2A, KAT2A), and PCAF (p300/CBP-associated factor, also known as KAT2B). Western blotting with anti-3K-Ac antibody showed that only GCN5 enhanced cavin-1 acetylation, whereas the other acetyltransferases had little effect on acetylation (Fig. 3A). Furthermore, overexpression of WT GCN5 but not the

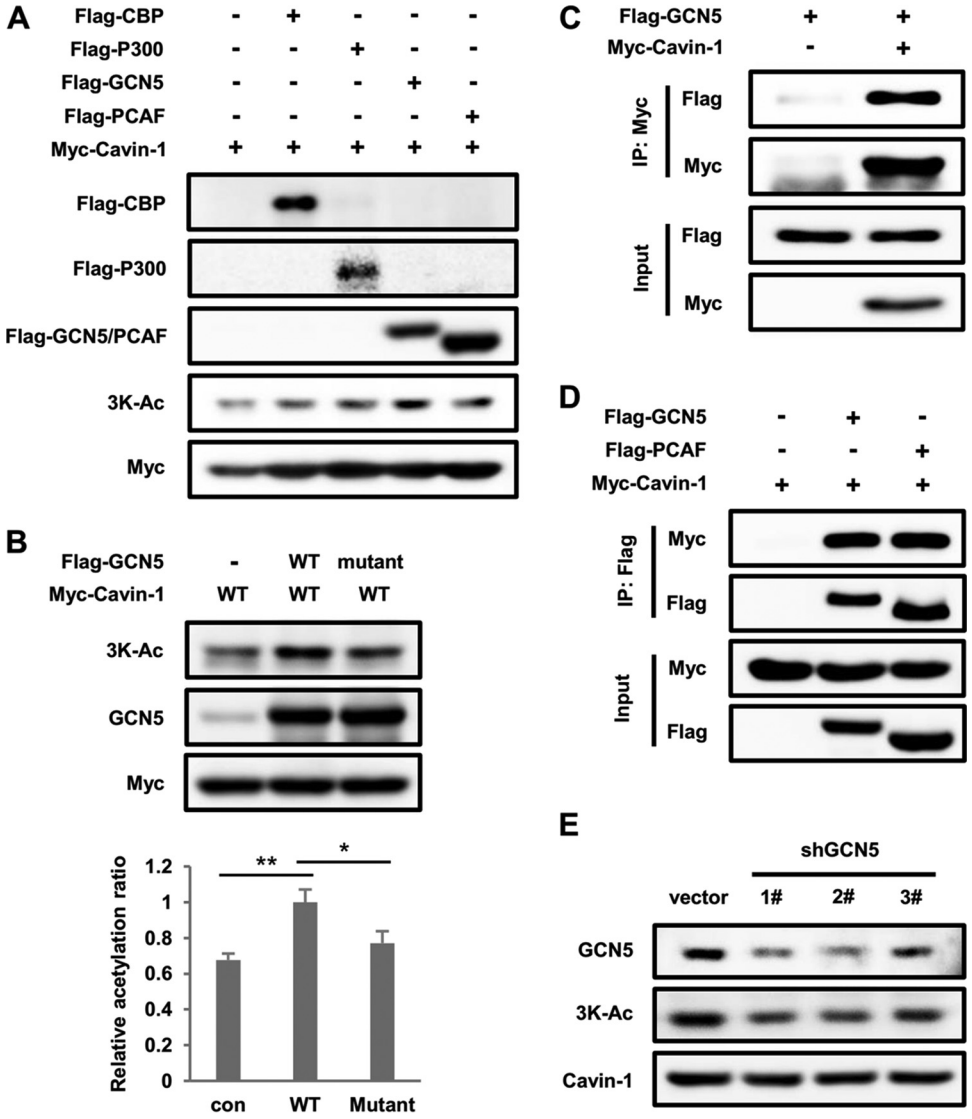

FIG 3 GCN5 enhances cavin-1 acetylation. (A) Overexpression of GCN5 but not other acetyltransferases increases cavin-1 acetylation at 3K. Myc-tagged cavin-1 was transfected into HEK293T cells with Flag-tagged CBP, P300, GCN5, or PCAF. Cavin-1 acetylation was measured by Western blotting with an anti-3K-Ac antibody. (B) A catalytically inactive GCN5 mutant does not acetylate cavin-1. HEK293T cells were transfected with the indicated plasmids, and acetylation levels of cavin-1 were analyzed by Western blotting. Relative acetylation/protein ratios were quantified. con, cotransfected with vector control; WT, cotransfected with wild-type GCN5; Mutant, cotransfected with the catalytically inactive GCN5 mutant. Error bars represent ±SD for experiments performed in triplicate. (C) GCN5 binds with cavin-1. Myc-tagged cavin-1 was cotransfected with Flag-tagged GCN5 into HEK293T cells and immunoprecipitated with an anti-Myc antibody. The presence of GCN5 in immunoprecipitates was determined by Western blotting with an antibody against Flag. (D) Cavin-1 coimmunoprecipitates with GCN5 and PCAF. The indicated plasmids were coexpressed into HEK293T cells, and the interactions of cavin-1 with GCN5 and PCAF were analyzed by immunoprecipitation and Western blotting. (E) GCN5 knockdown decreases endogenous cavin-1 acetylation at 3K. 3T3-L1 adipocytes were transduced with lentivirus-driven shGCN5 or control shRNA, and acetylation of endogenous cavin-1 was measured by Western blotting using an anti-3K-Ac antibody.

dominant-negative mutant GCN5 significantly increased 3K acetylation of cavin-1 (Fig. 3B). Additionally, cavin-1 and GCN5 coimmunoprecipitated when both were coexpressed in 293T cells (Fig. 3C and D). Notably, PCAF also interacted directly with cavin-1, indicating that PCAF may acetylate cavin-1 but not at 3K acetylation sites. GCN5 knockdown noticeably reduced 3K acetylation of endogenous cavin-1 in 3T3-L1 adipocytes (Fig. 3E), which indicates that GCN5 is the acetyltransferase responsible for 3K acetylation of cavin-1.

3K acetylation of cavin-1 recruits HSL to the plasma membrane by enhanced interaction. A previous study reported that cavin-1 and HSL are both translocated from

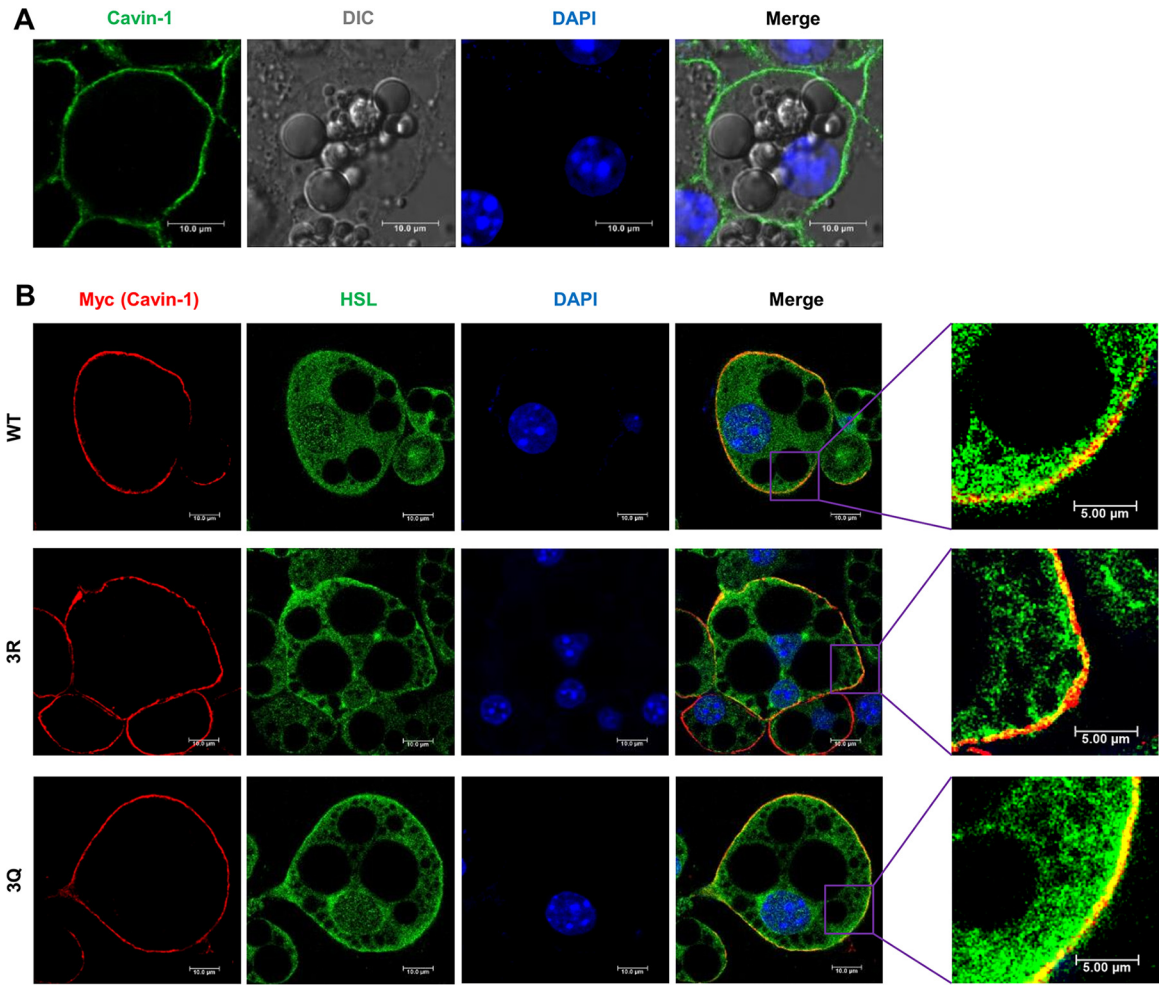

FIG 4 3K acetylation of cavin-1 recruits HSL to the plasma membrane. (A) Cavin-1 localizes in the plasma membrane of 3T3-L1 adipocytes. The subcellular localization of endogenous cavin-1 in 3T3-L1 adipocytes was examined by immunofluorescence using anti-cavin-1 antibodies. The nuclei were stained with DAPI. DIC, differential interference contrast. (B) 3K acetylation of cavin-1 recruits HSL to the plasma membrane. 3T3-L1 adipocytes were infected with recombinant adenovirus expressing Myc-tagged cavin-1^{WT}, cavin-1^{3R}, and cavin-1^{3Q}. The subcellular localization of Myc-cavin-1 (red) and endogenous HSL (green) was examined by immunofluorescence using anti-Myc and anti-HSL antibodies.

the plasma membrane to the cytosol in adipocytes in response to insulin (21). Therefore, we hypothesized that cavin-1 interacts with HSL in the plasma membrane in an acetylation-dependent manner. To address this issue, we first investigated whether cavin-1 acetylation would affect its subcellular localization. We expressed recombinant Myc-tagged WT, 3R (deacetylation-mimetic mutant), and 3Q (acetylation-mimetic mutant) cavin-1 in 3T3-L1 adipocytes using a recombinant adenovirus. Endogenous and exogenous (Myc-tagged WT, 3R, and 3Q) cavin-1 mostly localized in the plasma membrane in 3T3-L1 adipocytes (Fig. 4A and B) but not in the cytosol or nucleus in other cell lines, as previously reported (22). Notably, the expected colocalization of cavin-1 and HSL in the plasma membrane was evident, and acetylation-mimetic mutant (3Q) cavin-1 colocalized with HSL more strikingly than WT and deacetylation-mimetic mutant (3R) cavin-1 (Fig. 4B). Thus, cavin-1 may interact with HSL in the plasma membrane, which depends strongly on its acetylation level.

We next performed a series of coimmunoprecipitation experiments to investigate whether 3K acetylation contributes to the interaction between cavin-1 and HSL. Cavin-1 indeed coimmunoprecipitated with HSL in HEK293T cells (Fig. 5A), and HSL rather than ATGL showed high-affinity binding to cavin-1 (Fig. 5B). More importantly, we observed that the amount of HSL coimmunoprecipitated with cavin-1 significantly decreased in

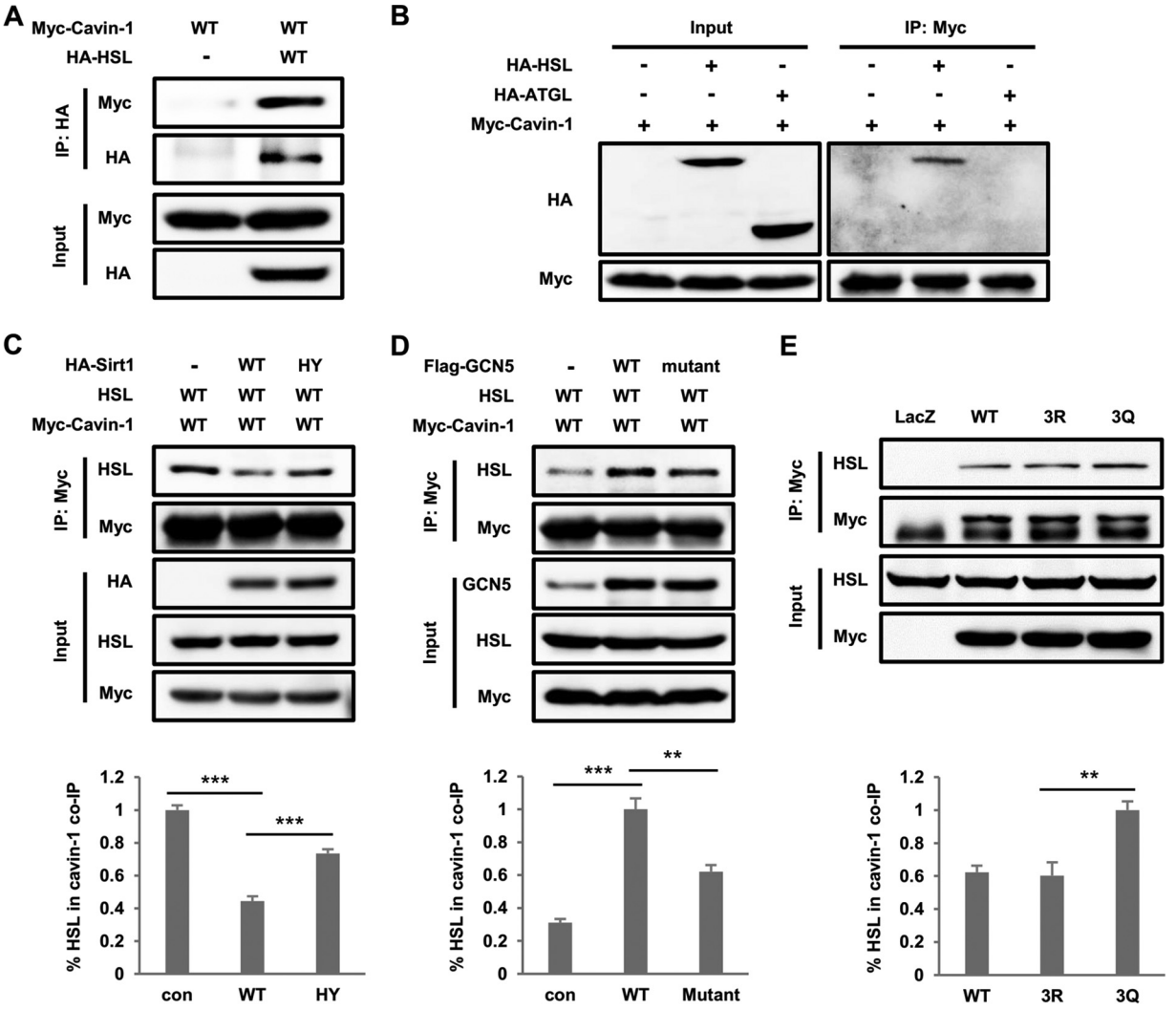

FIG 5 3K acetylation of cavin-1 enhances its interaction with HSL. (A) Cavin-1 coimmunoprecipitates with HSL. HEK293T cells were cotransfected with HA-tagged HSL and Myc-tagged cavin-1. HA-HSL was immunoprecipitated using an anti-HA antibody, and the presence of cavin-1 in precipitates was detected using an anti-Myc antibody. (B) HSL rather than ATGL binds with cavin-1. HA-tagged HSL and ATGL were individually cotransfected into HEK293T cells with Myc-tagged cavin-1. The binding between cavin-1 and HSL/ATGL were examined by immunoprecipitation and Western blot analysis. (C) Wild-type (WT) Sirt1, but not the catalytically inactive mutant HY, attenuates the interaction of cavin-1 and HSL. The plasmids were cotransfected into HEK293T cells as indicated. Myc-cavin-1 was immunoprecipitated and subjected to Western blotting with the indicated antibodies. (D) HSL preferentially interacts with 3K-acetylated cavin-1 acetylated by WT GCN5 but not the dominant-negative mutant. HEK293T cells were cotransfected with the indicated vectors, and protein interactions were determined by immunoprecipitation and Western blotting. (E) Acetyl mimetic 3Q mutation increases the binding between cavin-1 and endogenous HSL. 3T3-L1 adipocytes were infected with recombinant adenovirus expressing LacZ or Myc-tagged cavin-1. The binding between cavin-1 and HSL was examined by immunoprecipitation and Western blot analysis. The graphs at the bottom of panels C to E represent the amount of HSL coimmunoprecipitated with cavin-1 as a percentage of the total amount of HSL in inputs.

the cells expressing WT Sirt1 compared to cells expressing the vector or deacetylase-inactive mutant of Sirt1 (HY) (Fig. 5C). In contrast, cells expressing WT GCN5 and dominant-negative mutant GCN5 both promoted the binding of HSL and cavin-1 compared to control cells. However, cells expressing WT GCN5 enhanced the interaction more obviously than cells expressing the dominant-negative mutant GCN5 (Fig. 5D). In addition, endogenous HSL was more strongly bound to the acetylation-mimetic 3Q mutant than to WT cavin-1 in 3T3-L1 adipocytes (Fig. 5E), which further confirmed that acetylation of cavin-1 enhanced its interaction with HSL. Taken together, these data indicate that 3K acetylation of cavin-1 preferentially recruits HSL to the plasma membrane.

3Q mutant cavin-1 augments fat mobilization. Recently, cavin-1 has been reported to promote lipolysis in 3T3-L1 adipocytes (14, 15). To test the role of 3K

acetylation in lipolysis, 3T3-L1 adipocytes were infected with recombinant adenovirus expressing Myc-tagged cavin-1 (WT, 3R, and 3Q) and were left untreated or were treated with isoproterenol. Cavin-1 protein levels increased 2-fold compared with adipocytes infected with the control adenovirus carrying the *Escherichia coli* beta-galactosidase gene (*lacZ*), and it is noteworthy that isoproterenol could induce the stabilization of cavin-1 (Fig. 6A), as previously reported (15). Eight hours after isoproterenol treatment, cells expressing WT cavin-1 showed significantly more glycerol release than *lacZ*-infected cells. The 3Q mutant, but not the 3R mutant, further enhanced glycerol release compared to WT cavin-1 (Fig. 6B). These results suggest that cavin-1 increases lipolysis in an acetylation-dependent manner.

To determine whether 3K acetylation of cavin-1 affects lipid metabolism *in vivo*, we examined fat mobilization during fasting in transgenic zebrafish after heat shock-induced overexpression of WT or 3Q cavin-1. For this, we used the Tol2kit (23) to facilitate zebrafish transgenesis by assembling pDestTol2CG-*hsp70*-[cavin-1(WT/3Q)-EGFP]-polyA constructs in a Tol2 transposon backbone (Fig. 6C). Without heat shock, the transgenic zebrafish displayed green fluorescence only in the heart (Fig. 6D). However, heat-shocked transgenic zebrafish were globally green (Fig. 6D), and the fluorescence was observed continuously for at least 7 days (data not shown), indicating the ability of these constructs to successfully trigger conditional overexpression of WT or 3Q cavin-1.

We next tested the whole-body glycerol content to reflect the rate of fat mobilization in zebrafish in response to fasting. After 48 h of fasting, the total extracted glycerol levels were higher in heat-shocked 3Q transgenic zebrafish than in heat-shocked WT transgenic zebrafish (Fig. 6E). In contrast, whole-body glycerol levels were similar in WT and 3Q transgenic zebrafish fasted 48 h without heat shock, and levels in both of these groups were lower than those of heat-shocked transgenic zebrafish. To examine the ability of WT and 3Q zebrafish to mobilize fat depots, we fasted individual 1-month-postfertilization (mpf) zebrafish and monitored fat depots longitudinally using Nile red. After 5 days of fasting, Nile red staining revealed that fat depots of VAT, SAT, and miscellaneous adipose tissue (MAT) in heat-shocked WT and 3Q zebrafish were reduced in size (Fig. 6F). The reduction ratio of the VAT area during the 5 days of fasting was 52.92% in heat-shocked 3Q zebrafish, which was significantly higher than that in heat-shocked WT zebrafish (18.68%) (Fig. 6G). Similarly, according to microcomputed tomography (micro-CT) analysis, the volume of fat depots were decreased more obviously in heat-shocked 3Q zebrafish after 5 days of fasting (Fig. 6H and I). Histological analysis of VAT depots revealed that heat-shocked 3Q zebrafish contained significantly smaller amounts of lipids during fasting than heat-shocked WT zebrafish (Fig. 6J). Therefore, heat-shocked 3Q zebrafish have markedly different properties in lipid metabolism than heat-shocked WT zebrafish, and heat-shocked 3Q zebrafish undergo augmented fat mobilization during fasting.

3K acetylation of cavin-1 is under nutritional regulation. Protein acetylation is a reversible process involved in cellular metabolic status and levels of intermediary metabolites, such as NAD^+ and acetyl coenzyme A (CoA) (24). Therefore, we investigated the effect of different nutritional statuses on 3K acetylation levels of cavin-1. We treated 3T3-L1 adipocytes with low- or high-glucose medium for 3 h and found that high glucose significantly increased 3K acetylation of cavin-1 (Fig. 7A). Similarly, oleic acid treatment for 3 h resulted in a strong upregulation of cavin-1 acetylation, which was consistent with changes in protein expression of GCN5 and Sirt1 (Fig. 7B). We next detected the *in vivo* 3K acetylation levels of cavin-1 in WAT of C57BL/6 male mice under different nutritional statuses. Mice fasted for 48 h displayed an elevated level of cavin-1 acetylation owing to high expression of cavin-1 protein, with a moderate reduction in GCN5 expression and increase in Sirt1 expression (Fig. 7C). Additionally, we fed mice a high-fat diet (HFD) for 16 weeks and found that HFD treatment resulted in a robust increase in 3K acetylation of cavin-1 and expression of GCN5 in WAT compared to

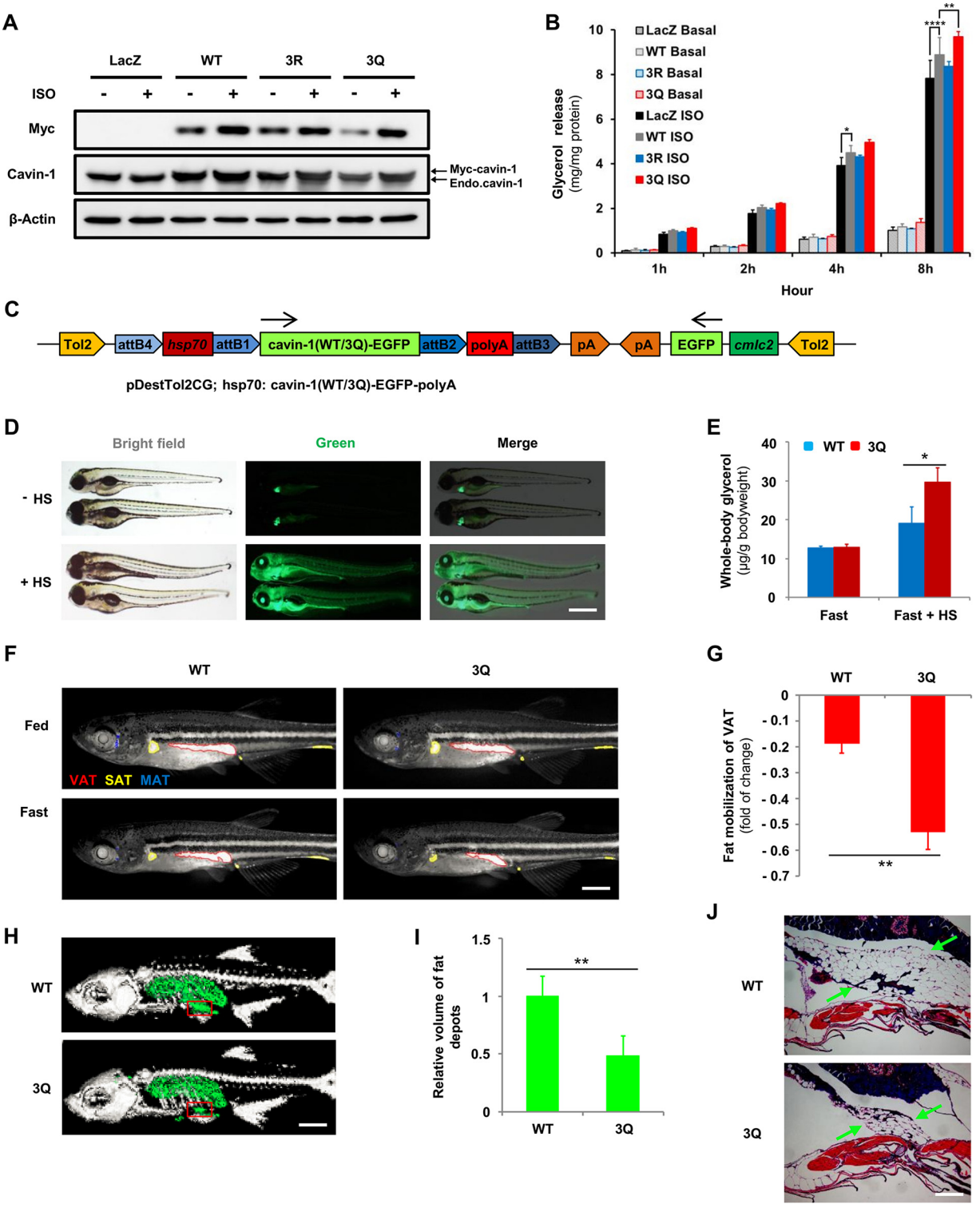

FIG 6 3Q mutant cavin-1 augments fat mobilization. (A and B) Cavin-1^{3Q} mutant promotes lipolysis. Myc-tagged cavin-1^{WT}, cavin-1^{3R}, and cavin-1^{3Q} were overexpressed in 3T3-L1 adipocytes by recombinant adenovirus with or without isoproterenol (ISO) treatment (10 μM) for the indicated times. (A) Protein levels of cavin-1 were determined by Western blotting using either an anti-Myc or an anti-cavin-1 antibody. (B) Basal and isoproterenol-stimulated glycerol release were measured and normalized to total cellular protein (n = 3 basal, n = 5 ISO). (C) Schematic diagram of expression construct showing the configuration of the pDestTol2CG-*hsp70*-[cavin-1(WT/3Q)-EGFP]-polyA plasmid used to generate wild-type (WT) and 3Q transgenic zebrafish. pDestTol2CG includes an extra *cmlc2*-EGFP-pA expression cassette, which drives expression of EGFP specifically in the heart. Arrows indicate the direction of transcription. (D) Test of pDestTol2CG destination vector. Embryos of F1 progenies were selected for green hearts at 30 h postfertilization (hpf). At 48 hpf, the transgenic embryos were left untreated or were treated with heat shock (HS) at 39°C for 15 min and imaged using a fluorescence stereomicroscope 2 h later. Scale bar, 500 μm. (E) Cavin-1^{3Q} increases lipolysis *in vivo* during fasting. Two months postfertilization (mpf), cavin-1^{WT} and cavin-1^{3Q} transgenic zebrafish were left untreated or were treated with HS at

(Continued on next page)

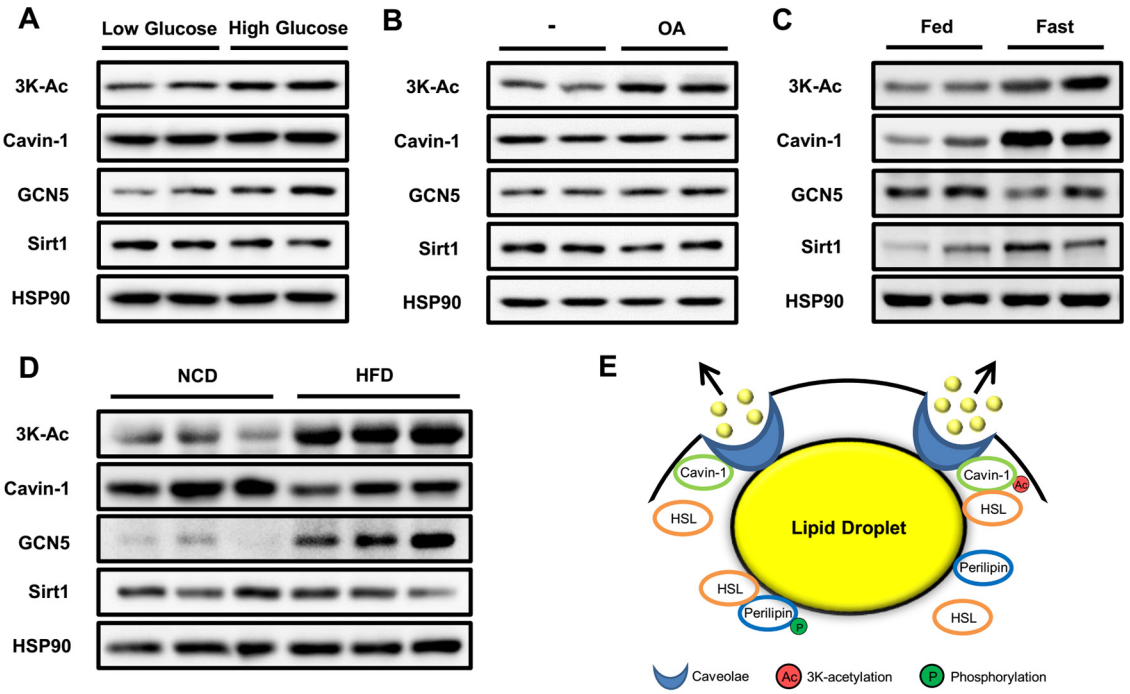

FIG 7 3K acetylation of cavin-1 is under nutritional regulation. (A and B) Glucose and fatty acids increase cavin-1 acetylation in 3T3-L1 adipocytes. Cells were incubated for 3 h in either low-glucose (5 mM) or high-glucose (25 mM) medium (A) or with 500 μM oleic acid (OA) (B) and subjected to Western blotting with the indicated antibodies. (C and D) 3K acetylation of cavin-1 in white adipose tissue is regulated by nutritional status. (C) C57BL/6 male mice at 20 weeks of age were fasted for 48 h. (D) C57BL/6 male mice at 4 weeks of age were fed with either a normal chow diet (NCD) or a high-fat diet (HFD) for 16 weeks. (E) A model for 3K acetylation of cavin-1 in regulating lipolysis as a reversible posttranslational modification in adipocytes. Cavin-1 acetylation promotes lipolysis by docking HSL at the surface of the caveolae in the plasma membrane.

normal chow diet (NCD) (Fig. 7D). From these results, we conclude that 3K acetylation of cavin-1 is regulated by nutritional status.

DISCUSSION

Dysregulation of lipolysis under different nutritional statuses can lead to a variety of metabolic disorders. Nutritional demand increases the release of FFAs into circulation from WAT, which provides an energy source for fatty acid β-oxidation in the liver and skeletal muscle. In the liver, however, rapid body fat mobilization induced by fasting results in excessive TAG accumulation and hepatic steatosis (25–27). Numerous studies have demonstrated that nutritional excess (such as HFD-induced obesity) is associated with enhanced adipose lipolysis (2, 28, 29), which further aggravates hyperlipidemia and the pathophysiology of obesity-associated metabolic disorders, including nonalcoholic fatty liver disease, type 2 diabetes, and atherosclerotic heart disease. Thus, regulation of lipolysis to maintain lipid homeostasis is critical in health and disease.

FIG 6 Legend (Continued)
39°C for 15 min and then fasted for 48 h. Whole-body glycerol content was measured and normalized to body weight ($n = 3$ fast, $n = 6$ fast + HS). (F and G) Cavin-1^{3Q} mutant promotes fat mobilization *in vivo*. One-month-postfertilization cavin-1^{WT} and cavin-1^{3Q} transgenic zebrafish were treated with HS at 39°C for 15 min and then fasted for 5 days. Individual zebrafish were stained with Nile red and imaged before and after 5 days of fasting to monitor neutral lipid deposits. (F) Fluorescent stereoscope images of Nile red-stained zebrafish were inverted and false colored according to visceral adipose tissue (VAT; red), subcutaneous adipose tissue (SAT; yellow), or miscellaneous adipose tissue (MAT; blue). Scale bar, 1,000 μm. (G) Reduction ratios of VAT area in cavin-1^{WT} and cavin-1^{3Q} zebrafish during 5 days of fasting ($n = 3$). (H to J) The cavin-1^{3Q} transgenic zebrafish show less fat volume during fasting. Two-month-postfertilization cavin-1^{WT} and cavin-1^{3Q} transgenic zebrafish were treated with HS at 39°C for 15 min and then fasted for 5 days. (H) Images show reconstructed three-dimensional tomographies of the cavin-1^{WT} and cavin-1^{3Q} transgenic zebrafish subjected to microcomputed tomography (CT) analysis. Bone is depicted in light gray, and fat depots are depicted in green. Scale bar, 2,000 μm. (I) Volumes of fat depots were determined by micro-CT for the entire body and normalized to body weight ($n = 4$). (J) Hematoxylin and eosin staining of the boxed region shown in panel H of cavin-1^{WT} and cavin-1^{3Q} transgenic zebrafish. Arrows indicate VAT. Scale bar, 250 μm. *, $P \leq 0.05$; **, $P \leq 0.01$; ***, $P \leq 0.001$.

Here, we report an essential role of cavin-1 acetylation in the regulation of lipid metabolism in WAT.

Cavin-1 resides on the cytoplasmic face of caveolae and is the major caveola-associated protein in primary human adipocytes (16). In the present study, we have uncovered a mechanism whereby cavin-1 regulates lipolysis in an acetylation-dependent manner (Fig. 7E). Acetylated cavin-1 preferentially interacted with HSL and recruited it to the caveolae, thereby promoting lipolysis. Since caveolae are omega-shaped invaginations of the plasma membrane in white adipocyte, which is almost occupied by one large lipid droplet, we hypothesize that the lipid droplet is near or in close contact with caveolae, which facilitates hydrolysis of TAG and release of FFA into circulation. In fact, a significant amount of *in vivo* and *in vitro* data support the hypothesis that caveolae play a protective role in modulating FFA trafficking in and out of adipocytes (30). Therefore, similar to the phosphorylation of perilipin that promotes translocation of HSL from the cytosol to the lipid droplets during catecholamine-stimulated lipolysis (31), 3K acetylation of cavin-1 can also dock HSL at the surface of the caveolae to increase lipid mobilization. Nonetheless, the precise mechanism by which the interaction between cavin-1 and HSL regulates lipolysis remains to be determined. A previous report showed that phosphorylation of cavin-1 is required for efficient fat mobilization (15), suggesting that cross talk between phosphorylation and acetylation exists. Stoeber et al. very recently reported that cavin-1 monomers form trimers and then assemble into larger, interconnected oligomers to form a dodecahedron around the caveolar membrane (32). In their speculative model, the C terminus of cavin-1 (amino acids 285 to 392), which contains the 3K acetylation sites, is free and external to the caveolar coat, indicating that 3K acetylation sites of cavin-1 are likely involved in the interaction with HSL. It also would be of interest to determine whether there are other important roles of HSL at the surface of the caveolae in the plasma membrane.

Cavin-1 expression in WAT is regulated by nutritional status, and this nutritional regulation is mediated directly by insulin and isoproterenol (15). Consistent with this, we found that isoproterenol and fasting both led to significant increases in cavin-1 protein levels (Fig. 6A and 7C) and that HFD treatment downregulated the expression of cavin-1 (Fig. 7D), possibly due to an increased plasma insulin level in mice fed an HFD (33). Similarly, 3K acetylation of cavin-1 is under nutritional regulation, which might play physiological and pathological roles in lipid metabolism under different nutritional statuses.

Lysine acetylation plays a major role in metabolic regulation (34). Our findings show that the 3K acetylation state of cavin-1 is modulated by the deacetylase Sirt1 and the acetyltransferase GCN5. The activities of both Sirt1 and GCN5 are dictated by the energy status of the cell due to their respective cosubstrates of NAD^+ and acetyl-CoA, which are directly involved in metabolism and energy sensing (35). Therefore, Sirt1 and GCN5 may enable cavin-1 acetylation to synchronize lipid homeostasis to the fluctuating nutritional status. It is possible that multiple defects in these nutritional signaling pathways cause abnormalities of lipid metabolism. Ultimately, a better understanding of how cavin-1 acetylation regulates lipid metabolism may help to design new therapeutic strategies to reverse metabolic disorders under different nutritional statuses.

MATERIALS AND METHODS

Zebrafish and mouse experiments. The AB strain zebrafish were raised, fed, and housed as described previously (36). To generate the transgenic zebrafish (WT/3Q), we used the Tol2kit system to facilitate the rapid, modular assembly of pDestTol2CG-hsp70-[cavin-1(WT/3Q)-EGFP]-polyA constructs in a Tol2 transposon backbone by site-specific recombination-based cloning (multisite gateway technology) (23). We selected the F1 progenies of transgenic zebrafish that displayed enhanced green fluorescent protein (EGFP) in the heart (the F1 progenies were derived from outcrossing with AB strain zebrafish). We then identified the selected zebrafish with globally green fluorescent signals after heat shock at 39°C for 15 min and confirmed the identification with DNA sequencing results.

Male C57BL/6 mice were purchased from the Model Animal Research Center of Nanjing University. All mice were either maintained in a temperature-controlled environment at 25°C under a 12-h light/12-h dark cycle with an NCD or housed under the previously stated conditions for fasting or HFD treatment.

All experiments were approved by the Animal Care and Use Committee of the Shanghai Medical College, Fudan University.

Cell culture and differentiation. The HEK293T and HEK293A cells were propagated and maintained in Dulbecco's modified Eagle medium (DMEM) containing 10% fetal bovine serum (FBS). The 3T3-L1 preadipocytes were cultured in DMEM with 10% newborn calf serum. Two days after reaching confluence, 3T3-L1 preadipocytes were differentiated into adipocytes with DMEM containing 10% FBS, 1 μM dexamethasone, 1 μg/ml insulin, and 0.5 mM isobutylmethylxanthine for 2 days. After this, the cells were cultured in medium containing 10% FBS and 1 μg/ml insulin for another 2 days. The 3T3-L1 adipocytes were fed every other day in DMEM with 10% FBS until harvest. For NAM and TSA treatments, cells were incubated with a final concentration of 20 mM NAM (Sigma) for 12 h and 0.5 μM TSA (Sigma) for 18 h.

Plasmids and antibodies. All plasmids were constructed using a standard PCR-based cloning technique from cDNA templates with different primer sets containing Myc, Flag, or HA sequences. The PCR products of target genes were cloned into the vector pcDNA3.1 and verified by DNA sequencing. Cavin-1, Sirt1, and GCN5 mutant forms were generated by site-directed mutagenesis through a standard PCR-based approach. Plasmid transfections were conducted with Lipofectamine 2000 (Invitrogen) according to the manufacturer's instructions. Antibodies against pan-acetyl lysine (ImmuneChem), Myc, Flag, HA (Earthox), cavin-1 (proteintech), HSL (Cell Signaling Technology), HSP90, GCN5 (Santa Cruz), Sirt1, and β-actin (Abcam) were purchased commercially. Antibodies specifically recognizing acetylation at lysines 291, 293, and 298 (anti-3K-Ac) of cavin-1 were generated commercially (Shanghai Genomics, Inc.) by immunizing rabbits.

Recombinant adenoviruses and lentivirus transduction. For overexpression of Myc-tagged cavin-1 (WT/3R/3Q) in 3T3-L1 adipocytes, we generated recombinant adenoviruses using the ViraPower adenoviral expression system (Invitrogen). For Sirt1 and GCN5 knockdown, we subcloned three anti-SIRT1 and anti-GCN5 short-hairpin RNA (shRNA) sequences into lentiviral vector pLKO.1 (Addgene). We used the following shRNA sequences: shSirt1, 5′-AAGTTGACCTCCTCATTGTTA-3′, 5′-AGTGAGACCAGTAG CACTAAT-3′, and 5′-CTAGACCAAAGAATGGTATTT-3′; and shGCN5, 5′-CAAGAAGTTGATTGAGCGCAA-3′, 5′-GCTACCTACAAAGTCAATTAT-3′, and 5′-GAAGCCTTCTACGGTCCATTT-3′. We added supernatants containing viral particles to 3T3-L1 adipocytes 5 days after differentiation. We studied the cells at 5 days postransduction.

Immunoprecipitation and immunoblotting. The cells and tissues were lysed on ice in radioimmunoprecipitation assay (RIPA) buffer (1% Triton X-100, 50 mM Tris [pH 7.4], 150 mM NaCl) containing 50 mM NAM and protease inhibitor mixture (Roche). For immunoprecipitation, cell lysates were incubated with the indicated antibodies overnight at 4°C and with protein G-agarose beads (Roche) for 3 h. The binding complexes were washed four times with RIPA buffer and then subjected to SDS-PAGE. For immunoblotting, equal amounts of protein were separated on SDS-PAGE, blotted onto a polyvinylidene difluoride membrane (Millipore), incubated with primary antibodies, and visualized with secondary antibodies conjugated to horseradish peroxidase.

Lipolysis assays. For basal and stimulated lipolysis, 3T3-L1 adipocytes were cultured in serum-free DMEM containing 2% bovine serum albumin (BSA) (Sigma) for 16 h and then treated with isoproterenol (Sigma) for the indicated times. For *in vivo* lipolysis of zebrafish, individual zebrafish were anesthetized by tricaine, snap-frozen, and homogenized in a 300-μl solution containing 5% NP-40 in water. Homogenates were slowly heated to 85°C in a water bath for 5 min and then centrifuged at 12,000 $\times$ *g* for 2 min to remove any insoluble material. We measured glycerol release using the free glycerol reagent kit (Sigma). Glycerol levels were normalized to total cellular protein or body weights of zebrafish.

Immunofluorescence microscopy. 3T3-L1 adipocytes were grown on coverslips, fixed in 4% polyformaldehyde (in phosphate-buffered saline [PBS]) for 10 min, and permeabilized with 0.2% Triton X-100 in PBS for 10 min. Cells were blocked with PBS containing 1% BSA for 1 h at room temperature, incubated with appropriate primary and secondary antibodies in 1% BSA, as indicated in the figure legends, and then mounted with 4′,6-diamidino-2-phenylindole (DAPI) (Sigma). Fluorescence images were scanned on a Leica confocal microscope (Leica TCS SP5).

Nile red staining. Nile red staining was performed as described previously (36). Live unanesthetized zebrafish were exposed to fish water containing 0.5 μg/ml Nile red in the dark at 28°C for 30 min and then rinsed with fish water for 1 min to reduce staining background. After being anesthetized with tricaine, the zebrafish were observed and imaged using a fluorescence stereomicroscope (Olympus SZX2-ILLB).

MS analysis. We conducted MS-based proteomic analyses to profile the acetylated proteins in adipose tissue according to a previously reported approach (18). We used centrifugation to separate the cellular fractions from SAT, VAT, and BAT into nuclear, mitochondrial, and cytosolic proteins. Proteins in each fraction were digested into peptides by sequencing-grade trypsin (Promega), and then acetylated peptides were enriched by incubation with agarose-conjugated acetyl lysine antibody (ImmuneChem) at 4°C. Enriched acetylated peptides were subjected to MS/MS analysis in an LTQ-Orbitrap mass spectrometer (Thermo Electron).

Micro-CT imaging. Zebrafish were fixed in 8% paraformaldehyde at 4°C overnight and embedded in 1.2% agarose gel, which was then placed on a radio-transparent bed. We imaged zebrafish using a Quantum GX micro-CT imaging system (PerkinElmer), which included an X-ray tube operating at 70 kV and 114 μA. Images were captured in the high-resolution mode with a 36-mm by 36-mm field of view and a 72-μm voxel size. Image reconstruction and fat determination were performed using advanced micro-CT analysis software of the Quantum GX system (PerkinElmer).

Statistical analysis. Statistical analyses were completed using a two-tailed unpaired Student *t* test. Results are presented as means $\pm$ standard deviations (SD) for at least three independent experiments.

Differences among more than two groups were assessed by analysis of variance, with *post hoc* analysis for multiple comparisons. *P* values of less than 0.05 were considered statistically significant.

SUPPLEMENTAL MATERIAL

Supplemental material for this article may be found at https://doi.org/10.1128/MCB.00058-17.

SUPPLEMENTAL FILE 1, XLSX file, 0.1 MB.

ACKNOWLEDGMENTS

We appreciate Yu-Xiao Yao and Shao-Yang Sun for assistance with zebrafish transgenesis. We thank Wen-Yan Jiang for her critical comments and suggestions on the working model (Fig. 7E).

This work was partially supported by National Key Basic Research Project grants 2011CB910201 and 2013CB530601, National Natural Science Foundation of China grants 81390350 and 31571471 (to Q.-Q.T.), National Natural Science Foundation of China grant 31370027 (to L.G.), and National Natural Science Foundation of China grant 81601251 (to Y.L.). The department is supported by Shanghai Leading Academic Discipline Project B110 and 985 Project 985 III-YFX0302.

REFERENCES

1. Attie AD, Scherer PE. 2009. Adipocyte metabolism and obesity. J Lipid Res 50(Suppl):S395–S399. https://doi.org/10.1194/jlr.R800057-JLR200.
2. Guilherme A, Virbasius JV, Puri V, Czech MP. 2008. Adipocyte dysfunctions linking obesity to insulin resistance and type 2 diabetes. Nat Rev Mol Cell Biol 9:367–377. https://doi.org/10.1038/nrm2391.
3. Samuel VT, Shulman GI. 2012. Mechanisms for insulin resistance: common threads and missing links. Cell 148:852–871. https://doi.org/10.1016/j.cell.2012.02.017.
4. Pilch PF, Liu L. 2011. Fat caves: caveolae, lipid trafficking and lipid metabolism in adipocytes. Trends Endocrinol Metab 22:318–324. https://doi.org/10.1016/j.tem.2011.04.001.
5. Hill MM, Bastiani M, Luetterforst R, Kirkham M, Kirkham A, Nixon SJ, Walser P, Abankwa D, Oorschot VM, Martin S, Hancock JF, Parton RG. 2008. PTRF-Cavin, a conserved cytoplasmic protein required for caveola formation and function. Cell 132:113–124. https://doi.org/10.1016/j.cell.2007.11.042.
6. Liu L, Brown D, McKee M, Lebrasseur NK, Yang D, Albrecht KH, Ravid K, Pilch PF. 2008. Deletion of Cavin/PTRF causes global loss of caveolae, dyslipidemia, and glucose intolerance. Cell Metab 8:310–317. https://doi.org/10.1016/j.cmet.2008.07.008.
7. Hayashi YK, Matsuda C, Ogawa M, Goto K, Tominaga K, Mitsuhashi S, Park YE, Nonaka I, Hino-Fukuyo N, Haginoya K, Sugano H, Nishino I. 2009. Human PTRF mutations cause secondary deficiency of caveolins resulting in muscular dystrophy with generalized lipodystrophy. J Clin Investig 119:2623–2633. https://doi.org/10.1172/JCI38660.
8. Dwianingsih EK, Takeshima Y, Itoh K, Yamauchi Y, Awano H, Malueka RG, Nishida A, Ota M, Yagi M, Matsuo M. 2010. A Japanese child with asymptomatic elevation of serum creatine kinase shows PTRF-CAVIN mutation matching with congenital generalized lipodystrophy type 4. Mol Genet Metab 101:233–237. https://doi.org/10.1016/j.ymgme.2010.06.016.
9. Rajab A, Straub V, McCann LJ, Seelow D, Varon R, Barresi R, Schulze A, Lucke B, Lutzkendorf S, Karbasiyan M, Bachmann S, Spuler S, Schuelke M. 2010. Fatal cardiac arrhythmia and long-QT syndrome in a new form of congenital generalized lipodystrophy with muscle rippling (CGL4) due to PTRF-CAVIN mutations. PLoS Genet 6:e1000874. https://doi.org/10.1371/journal.pgen.1000874.
10. Shastry S, Delgado MR, Dirik E, Turkmen M, Agarwal AK, Garg A. 2010. Congenital generalized lipodystrophy, type 4 (CGL4) associated with myopathy due to novel PTRF mutations. Am J Med Genet A 152A:2245–2253. https://doi.org/10.1002/ajmg.a.33578.
11. Ardissone A, Bragato C, Caffi L, Blasevich F, Maestrini S, Bianchi ML, Morandi L, Moroni I, Mora M. 2013. Novel PTRF mutation in a child with mild myopathy and very mild congenital lipodystrophy. BMC Med Genet 14:89. https://doi.org/10.1186/1471-2350-14-89.
12. Murakami N, Hayashi YK, Oto Y, Shiraishi M, Itabashi H, Kudo K, Nishino I, Nonaka I, Nagai T. 2013. Congenital generalized lipodystrophy type 4 with muscular dystrophy: clinical and pathological manifestations in early childhood. Neuromusc Disord 23:441–444. https://doi.org/10.1016/j.nmd.2013.02.005.
13. Jelani M, Ahmed S, Almramhi MM, Mohamoud HS, Bakur K, Anshasi W, Wang J, Al-Aama JY. 2015. Novel nonsense mutation in the PTRF gene underlies congenital generalized lipodystrophy in a consanguineous Saudi family. Eur J Med Genet 58:216–221. https://doi.org/10.1016/j.ejmg.2015.02.002.
14. Ding SY, Lee MJ, Summer R, Liu L, Fried SK, Pilch PF. 2014. Pleiotropic effects of cavin-1 deficiency on lipid metabolism. J Biol Chem 289:8473–8483. https://doi.org/10.1074/jbc.M113.546242.
15. Aboulaich N, Chui PC, Asara JM, Flier JS, Maratos-Flier E. 2011. Polymerase I and transcript release factor regulates lipolysis via a phosphorylation-dependent mechanism. Diabetes 60:757–765. https://doi.org/10.2337/db10-0744.
16. Aboulaich N, Vainonen JP, Stralfors P, Vener AV. 2004. Vectorial proteomics reveal targeting, phosphorylation and specific fragmentation of polymerase I and transcript release factor (PTRF) at the surface of caveolae in human adipocytes. Biochem J 383:237–248. https://doi.org/10.1042/BJ20040647.
17. Wang Q, Zhang Y, Yang C, Xiong H, Lin Y, Yao J, Li H, Xie L, Zhao W, Yao Y, Ning ZB, Zeng R, Xiong Y, Guan KL, Zhao S, Zhao GP. 2010. Acetylation of metabolic enzymes coordinates carbon source utilization and metabolic flux. Science 327:1004–1007. https://doi.org/10.1126/science.1179687.
18. Guan KL, Yu W, Lin Y, Xiong Y, Zhao S. 2010. Generation of acetyllysine antibodies and affinity enrichment of acetylated peptides. Nat Protoc 5:1583–1595. https://doi.org/10.1038/nprot.2010.117.
19. Shahbazian MD, Grunstein M. 2007. Functions of site-specific histone acetylation and deacetylation. Annu Rev Biochem 76:75–100. https://doi.org/10.1146/annurev.biochem.76.052705.162114.
20. Verdin E. 2014. The many faces of sirtuins: coupling of NAD metabolism, sirtuins and lifespan. Nat Med 20:25–27. https://doi.org/10.1038/nm.3447.
21. Aboulaich N, Ortegren U, Vener AV, Stralfors P. 2006. Association and insulin regulated translocation of hormone-sensitive lipase with PTRF. Biochem Biophys Res Commun 350:657–661. https://doi.org/10.1016/j.bbrc.2006.09.094.
22. Bai L, Deng X, Li J, Wang M, Li Q, An W, Deli A, Cong YS. 2011. Regulation of cellular senescence by the essential caveolar component PTRF/Cavin-1. Cell Res 21:1088–1101. https://doi.org/10.1038/cr.2011.56.
23. Kwan KM, Fujimoto E, Grabher C, Mangum BD, Hardy ME, Campbell DS, Parant JM, Yost HJ, Kanki JP, Chien CB. 2007. The Tol2kit: a multisite gateway-based construction kit for Tol2 transposon transgenesis constructs. Dev Dyn 236:3088–3099. https://doi.org/10.1002/dvdy.21343.
24. Menzies KJ, Zhang H, Katsyuba E, Auwerx J. 2016. Protein acetylation in metabolism–metabolites and cofactors. Nat Rev Endocrinol 12:43–60. https://doi.org/10.1038/nrendo.2015.181.

25. Guan HP, Goldstein JL, Brown MS, Liang G. 2009. Accelerated fatty acid oxidation in muscle averts fasting-induced hepatic steatosis in SJL/J mice. J Biol Chem 284:24644–24652. https://doi.org/10.1074/jbc.M109.034397.
26. Rouvinen-Watt K, Mustonen AM, Conway R, Pal C, Harris L, Saarela S, Strandberg U, Nieminen P. 2010. Rapid development of fasting-induced hepatic lipidosis in the American mink (Neovison vison): effects of food deprivation and re-alimentation on body fat depots, tissue fatty acid profiles, hematology and endocrinology. Lipids 45:111–128. https://doi.org/10.1007/s11745-009-3377-4.
27. Xu J, Donepudi AC, Moscovitz JE, Slitt AL. 2013. Keap1-knockdown decreases fasting-induced fatty liver via altered lipid metabolism and decreased fatty acid mobilization from adipose tissue. PLoS One 8:e79841. https://doi.org/10.1371/journal.pone.0079841.
28. Gaidhu MP, Anthony NM, Patel P, Hawke TJ, Ceddia RB. 2010. Dysregulation of lipolysis and lipid metabolism in visceral and subcutaneous adipocytes by high-fat diet: role of ATGL, HSL, and AMPK. Am J Physiol Cell Physiol 298:C961–C971. https://doi.org/10.1152/ajpcell.00547.2009.
29. Langin D, Dicker A, Tavernier G, Hoffstedt J, Mairal A, Ryden M, Arner E, Sicard A, Jenkins CM, Viguerie N, van Harmelen V, Gross RW, Holm C, Arner P. 2005. Adipocyte lipases and defect of lipolysis in human obesity. Diabetes 54:3190–3197. https://doi.org/10.2337/diabetes.54.11.3190.
30. Pilch PF, Meshulam T, Ding S, Liu L. 2011. Caveolae and lipid trafficking in adipocytes. Clin Lipidol 6:49–58.
31. Sztalryd C, Xu G, Dorward H, Tansey JT, Contreras JA, Kimmel AR, Londos C. 2003. Perilipin A is essential for the translocation of hormone-sensitive lipase during lipolytic activation. J Cell Biol 161:1093–1103. https://doi.org/10.1083/jcb.200210169.
32. Stoeber M, Schellenberger P, Siebert CA, Leyrat C, Helenius A, Grunewald K. 2016. Model for the architecture of caveolae based on a flexible, net-like assembly of Cavin1 and Caveolin discs. Proc Natl Acad Sci U S A 113:E8069–E8078. https://doi.org/10.1073/pnas.1616838113.
33. Winzell MS, Ahren B. 2004. The high-fat diet-fed mouse: a model for studying mechanisms and treatment of impaired glucose tolerance and type 2 diabetes. Diabetes 53(Suppl 3):S215–S219. https://doi.org/10.2337/diabetes.53.suppl_3.S215.
34. Zhao S, Xu W, Jiang W, Yu W, Lin Y, Zhang T, Yao J, Zhou L, Zeng Y, Li H, Li Y, Shi J, An W, Hancock SM, He F, Qin L, Chin J, Yang P, Chen X, Lei Q, Xiong Y, Guan KL. 2010. Regulation of cellular metabolism by protein lysine acetylation. Science 327:1000–1004. https://doi.org/10.1126/science.1179689.
35. Jeninga EH, Schoonjans K, Auwerx J. 2010. Reversible acetylation of PGC-1: connecting energy sensors and effectors to guarantee metabolic flexibility. Oncogene 29:4617–4624. https://doi.org/10.1038/onc.2010.206.
36. Minchin JE, Rawls JF. 2011. In vivo analysis of white adipose tissue in zebrafish. Methods Cell Biol 105:63–86. https://doi.org/10.1016/B978-0-12-381320-6.00003-5.